

Low-mass extension of direct detection bounds on WIMP-quark and WIMP-gluon effective interactions using the Migdal effect

Gaurav Tomar

*Physik-Department, Technische Universität München,
James-Frank-Straße, 85748 Garching, Germany*

Sunghyun Kang, Stefano Scopel

Department of Physics, Sogang University, Seoul, Korea, 121-742

Abstract

Updating a previous analysis where we used elastic nuclear recoils we study the Migdal effect to extend to low WIMP masses the direct detection bounds to operators up to dimension 7 of the relativistic effective field theory describing WIMP interactions with quarks and gluons. To this aim we include in our analysis the data of the XENON1T, SuperCDMS, COSINE-100, and DarkSide-50 experiments and assume a standard Maxwellian for the WIMP velocity distribution. We find that the bounds can reach down to a WIMP mass $\simeq 20$ MeV, although in the case of higher-dimension operators the energy scale of the ensuing constraints may be inconsistent with the validity of the effective theory.

1. Introduction

A worldwide effort has been under way for more than thirty years in the attempt to observe the interactions between the Weakly Interacting Massive Particles (WIMPs) expected to form the Dark Halo of our Galaxy and the nuclear targets of solid-state, liquid, and gaseous detectors appropriately shielded by cosmic rays in Direct Detection (DD) experiments run in underground laboratories around the world [1, 2].

The non-observation of new physics at the Large Hadron Collider (LHC) has increasingly constrained the most popular Dark Matter (DM) candidates predicted by extensions of the Standard Model (SM), prompting the need to use bottom-up approaches where the WIMP-nucleus interaction is parameterized in a model-independent way making use of effective models. A popular approach is to parameterize the WIMP interaction in terms of the most general relativistically-invariant WIMP-quark and WIMP-gluon operators up to some dimension [3],

$$\mathcal{L}_\chi = \sum_q \sum_{a,d} c_{a,q}^{(d)} \mathcal{O}_{a,q}^{(d)} + \sum_{b,d} c_b^{(d)} \mathcal{O}_b^{(d)}, \quad (1)$$

Email addresses: physics.tomar@tum.de (Gaurav Tomar), francis735@naver.com (Sunghyun Kang), scopel@sogang.ac.kr (Stefano Scopel)

with $C_{a,q}^{(d)}$ and $C_b^{(d)}$ some dimensional Wilson coefficients, and d the dimensionality of each operator.

In particular, in a previous analysis [4] we parameterized the Wilson coefficients C in terms of an effective scale $\tilde{\Lambda}$,

$$C_{a,q}^{(d)}, C_b^{(d)} = \frac{1}{\tilde{\Lambda}^{d-4}}, \quad (2)$$

and derived the bounds on $\tilde{\Lambda}$ from an extensive list of DD experiments searching for WIMP–nucleus recoils for each of the relativistic operators, $\mathcal{O}_{a,q}^{(d)}$, $\mathcal{O}_b^{(d)}$ up to $d=7$ listed in Eqs. (6-8), assuming a standard Maxwellian velocity distribution for the WIMPs in the halo of our Galaxy.

The bounds derived in the analysis of Ref. [4] were restricted to a WIMP mass $m_\chi \gtrsim 600$ MeV. Such loss of sensitivity at low WIMP mass is an intrinsic limitation of nuclear recoil searches, because in such process when m_χ is too low the minimal amount of energy deposited in the detector by the recoiling nucleus can exceed the experimental threshold of existing experiments only for an incoming WIMP speed larger than the escape velocity in the halo of our Galaxy.

As first pointed out in [5, 6, 7, 8] the production of nuclear excited states triggered by WIMP scattering can produce peculiar experimental signatures and, in particular, the sensitivity of direct detection experiments can be extended to lower WIMP masses [9, 10] by making use of the Migdal effect [11] in which the WIMP scattering process triggers the ionization of the recoiling nucleus. This is due to the fact that the ionization or excitation of an electron from an inner orbital can result in extra electronic energy injections, allowing to extend the experimental sensitivity below the threshold for elastic WIMP–nucleus scattering processes. Several experimental collaborations have exploited the Migdal effect in recent studies [12, 13, 14, 15, 16, 17, 18, 19]. The effect has been explored in great details for the standard WIMP interactions with ordinary matter [20, 21, 22, 23, 24, 25, 26, 27, 28, 29, 30, 31, 32], including non-standard WIMP-nucleon interactions using effective field theory (EFT) [33]. However, the analysis presented in [33] is limited as only four non-relativistic operators— \mathcal{O}_1 , \mathcal{O}_4 , \mathcal{O}_6 , \mathcal{O}_{10} —have been considered out of 14 different operators possible for spin-1/2 DM. Specifically, all the velocity-dependent operators have been left out. In the present work we analysed relativistic effective interactions which, in their non-relativistic limit, extend to non-relativistic operators not limited to \mathcal{O}_1 , \mathcal{O}_4 , \mathcal{O}_6 , \mathcal{O}_{10} , and contain a more broader picture of the Migdal effect in effective field theories.

The goal of the present letter is to use the Migdal effect to extend to $m_\chi \lesssim 600$ MeV the bounds discussed in Ref. [4] on the effective operators of Eq. (1). To this aim we will consider the dedicated analyses on the Migdal effect from four direct detection experiments: XENON1T [15], COSINE-100 [16], SuperCDMS [18], and DarkSide-50 [19]. Our main results are given in the exclusion plots of Figs. 2, 3 and 4.

The paper is organised as follows. In Section 2 we outline the procedure to calculate the expected rate for Migdal events triggered by WIMP–nucleus scattering; in Section 3 we summarize the effective models considered in the present analysis and already studied in Ref. [4]. Finally, we provide our quantitative results in Section 4 and our conclusions in Section 5.

2. Expected rates

In the Migdal effect the WIMP–nucleus scattering process is accompanied by the ejection of an electron from the recoiling nucleus with the ensuing deposit of an electromagnetic (EM)

signal in the detector. As a consequence, the techniques developed to discriminate between nuclear recoil processes and EM energy depositions are not applied, since the latter, rather than being only due to background, are produced also by WIMPs. This requires to re-analyze the experimental data and allows to lower the threshold compared to the analyses that look for elastic recoils. In particular, the ionisation event rate in an experiment due to the Migdal effect is calculated as [10],

$$\frac{dR}{dE_{det}} = \int_0^\infty dE_R \int_{v_{\min}(E_R)}^\infty dv_T \frac{d^3 R_{\chi T}}{dE_R dv_T dE_{det}} \quad (3)$$

with

$$\frac{d^3 R_{\chi T}}{dE_R dE_{det} dv_T} = \frac{d^2 R_{\chi T}}{dE_R dv_T} \times \frac{1}{2\pi} \sum_{n,l} \frac{d}{dE_e} p_{qe}^c(nl \rightarrow (E_e)). \quad (4)$$

The Migdal effect is usually negligible compared to the standard signal from elastic nuclear recoils, unless for very low WIMP masses for which the latter is below threshold. At higher WIMP masses a transition between Migdal and nuclear recoil takes place, until eventually the latter dominates. For the WIMP masses, target nuclei and the intervals for detected energy, E_{det} considered in the analysis of Section 4, we have verified that the EM energy produced by the recoil of the nucleus during the Migdal process remains negligible¹ In this case, neglecting the contribution from the nuclear recoil, $E_{det} \simeq E_{EM}$, where the total injected EM energy, E_{EM} is the sum of the outgoing electron energy, E_e and of the energy from de-excitation E_{nl} , where n and l are the initial quantum numbers of the ionized electron². Moreover, in Eqs. (3, 4) E_R is the nuclear recoil energy, v_T is the WIMP speed in the reference frame of the nuclear center of mass and,

$$v_{\min}(E_R) = \frac{m_T E_R + \mu_T E_{EM}}{\mu_T \sqrt{2m_T E_R}}. \quad (5)$$

In the above equation, m_T is the nucleus mass and μ_T represents the reduced mass. Finally p_{qe}^c represents the ionisation probability, while $q_e = m_e \sqrt{2E_R/m_T}$ is the average momentum transfer to an individual electron in the rest frame of the target nucleus.

In particular in our calculation we obtain the differential scattering rate spectrum $\frac{d^2 R_{\chi T}}{dE_R dv_T}$ using the WimPyDD [37] code, and utilise the ionization probabilities p_{qe}^c calculated in Ref. [10].

In our analysis we have followed the approach of XENON1T, DarkSide-50, SuperCDMS, and COSINE-100 adopting the isolated atom approximation, which is valid for inner shell electrons, neglecting the contribution from valence electrons. In particular, for solid-state detectors, as pointed out in [16, 18] most of the valence shell electrons contribution to the signal is below the experimental threshold, so that neglecting it implies a negligible decrease in the expected rate.

¹One exception is sodium, for which the effect of nuclear recoil is non-negligible in the interval of E_{det} used by COSINE-100 if a standard value found in the literature for the quenching factor, $q_{Na} = 0.3$, is used [34, 35]. However, in our analysis we use for sodium the quenching factor measured by COSINE-100 [36], that is significantly smaller. In this case the effect of nuclear recoil can be neglected.

²For this reason in the following E_{det} will be identified with E_{EM} .

3. Relativistic effective models

In this Section we outline the procedure that we follow to obtain the numerical results of Section 4. For definiteness, in our analysis we closely follow for the effective operators the notations of [3, 38], used also in [4]. In particular, we consider the two dimension-five operators,

$$\mathcal{Q}_1^{(5)} = \frac{e}{8\pi^2} (\bar{\chi} \sigma^{\mu\nu} \chi) F_{\mu\nu}, \quad \mathcal{Q}_2^{(5)} = \frac{e}{8\pi^2} (\bar{\chi} \sigma^{\mu\nu} i \gamma_5 \chi) F_{\mu\nu}, \quad (6)$$

where $F_{\mu\nu}$ is the electromagnetic field strength tensor and χ is the DM field, assumed here to be a Dirac particle. Such operators correspond, respectively, to magnetic–dipole and electric–dipole DM and imply a long–range interaction [39]. The dimension-six operators are,

$$\begin{aligned} \mathcal{Q}_{1,q}^{(6)} &= (\bar{\chi} \gamma_\mu \chi) (\bar{q} \gamma^\mu q), \quad \mathcal{Q}_{2,q}^{(6)} = (\bar{\chi} \gamma_\mu \gamma_5 \chi) (\bar{q} \gamma^\mu q), \\ \mathcal{Q}_{3,q}^{(6)} &= (\bar{\chi} \gamma_\mu \chi) (\bar{q} \gamma^\mu \gamma_5 q), \quad \mathcal{Q}_{4,q}^{(6)} = (\bar{\chi} \gamma_\mu \gamma_5 \chi) (\bar{q} \gamma^\mu \gamma_5 q). \end{aligned} \quad (7)$$

In our analysis we also consider the following dimension-seven operators,

$$\begin{aligned} \mathcal{Q}_1^{(7)} &= \frac{\alpha_s}{12\pi} (\bar{\chi} \chi) G^{a\mu\nu} G_{\mu\nu}^a, \quad \mathcal{Q}_2^{(7)} = \frac{\alpha_s}{12\pi} (\bar{\chi} i \gamma_5 \chi) G^{a\mu\nu} G_{\mu\nu}^a, \\ \mathcal{Q}_3^{(7)} &= \frac{\alpha_s}{8\pi} (\bar{\chi} \chi) G^{a\mu\nu} \tilde{G}_{\mu\nu}^a, \quad \mathcal{Q}_4^{(7)} = \frac{\alpha_s}{8\pi} (\bar{\chi} i \gamma_5 \chi) G^{a\mu\nu} \tilde{G}_{\mu\nu}^a, \\ \mathcal{Q}_{5,q}^{(7)} &= m_q (\bar{\chi} \chi) (\bar{q} q), \quad \mathcal{Q}_{6,q}^{(7)} = m_q (\bar{\chi} i \gamma_5 \chi) (\bar{q} q), \\ \mathcal{Q}_{7,q}^{(7)} &= m_q (\bar{\chi} \chi) (\bar{q} i \gamma_5 q), \quad \mathcal{Q}_{8,q}^{(7)} = m_q (\bar{\chi} i \gamma_5 \chi) (\bar{q} i \gamma_5 q), \\ \mathcal{Q}_{9,q}^{(7)} &= m_q (\bar{\chi} \sigma^{\mu\nu} \chi) (\bar{q} \sigma_{\mu\nu} q), \quad \mathcal{Q}_{10,q}^{(7)} = m_q (\bar{\chi} i \sigma^{\mu\nu} \gamma_5 \chi) (\bar{q} \sigma_{\mu\nu} q). \end{aligned} \quad (8)$$

Here, $q = u, d, s$ denote the light quarks, $G_{\mu\nu}^a$ is the QCD field strength tensor, while $\tilde{G}_{\mu\nu} = \frac{1}{2} \epsilon_{\mu\nu\rho\sigma} G^{\rho\sigma}$ is its dual, and $a = 1, \dots, 8$ are the adjoint color indices. For all the operators of Eqs.(6–8) we assume flavor conservation.

The detailed expression for the calculation of the differential rate $\frac{d^2 R_{\chi T}}{dE_R dv_T}$ in Eq. (4) is provided in Section 2 of [40], which has been implemented in the WimPyDD code [37]. In particular, in the non-relativistic limit the differential cross section is proportional to the squared amplitude,

$$\frac{d\sigma_T}{dE_R} = \frac{2m_T}{4\pi v_T^2} \left[\frac{1}{2j_\chi + 1} \frac{1}{2j_T + 1} |\mathcal{M}_T|^2 \right], \quad (9)$$

with m_T the nuclear mass, j_T, j_χ the spins of the target nucleus and of the WIMP, where $j_\chi = 1/2$, and [41],

$$\frac{1}{2j_\chi + 1} \frac{1}{2j_T + 1} |\mathcal{M}_T|^2 = \frac{4\pi}{2j_T + 1} \sum_{\tau=0,1} \sum_{\tau'=0,1} \sum_k R_k^{\tau\tau'} \left[c_i^\tau, c_j^{\tau'}, (v_T^\perp)^2, \frac{q^2}{m_N^2} \right] W_{Tk}^{\tau\tau'}(y). \quad (10)$$

In the above expression the squared amplitude $|\mathcal{M}_T|^2$ is summed over initial and final spins, the $R_k^{\tau\tau'}$'s are WIMP response functions which depend on the couplings c_j^τ as well as the transferred momentum \vec{q} , while,

$$(v_T^\perp)^2 = \frac{v_T^2 - v_{min}^2}{4}, \quad (11)$$

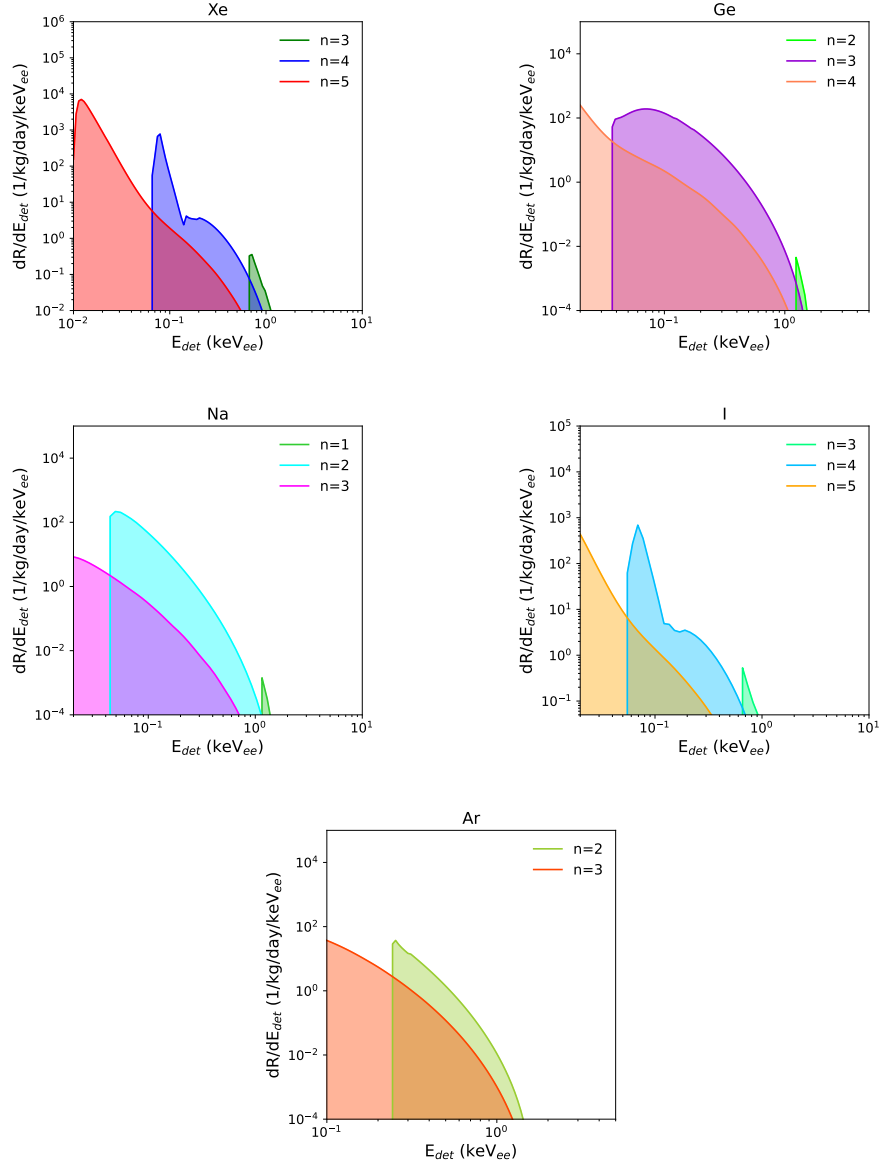


Figure 1: The Migdal differential rate for $m_\chi = 0.5$ GeV, taking $\tilde{\Lambda} = 1$ GeV and magnetic dipolar interaction $Q_1^{(5)}$, with Xe, Ge, Na, I, and Ar targets. In the horizontal axis the energy E_{det} includes the contribution to the deposited EM energy from nuclear recoils, which is only relevant above the threshold for elastic scattering events. When scattering events are below such threshold their contribution is negligible and $E_{det} \simeq E_{EM}$. The different color shadings correspond to the ionisation rates from $n = 1, 2, 3, 4,$ and 5 depending upon the considered targets.

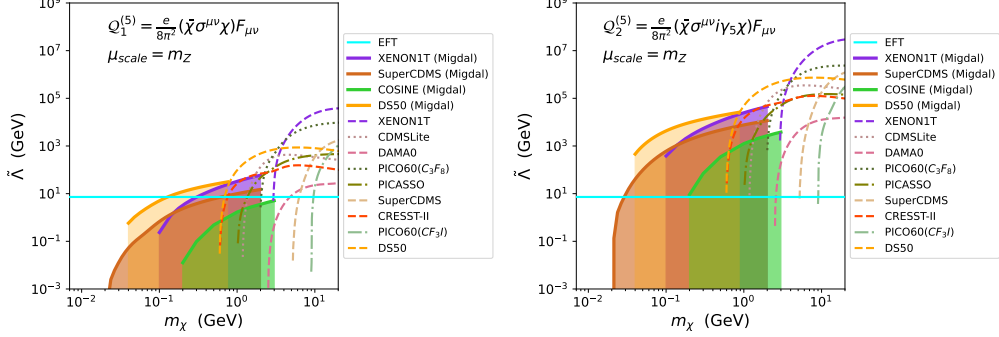


Figure 2: Lower bound on the effective scale $\tilde{\Lambda}$ for the operators $Q_{1,q}^{(5)}$ (left) and $Q_{2,q}^{(5)}$ (right). We fixed the dimensional couplings $C_{1,q}^{(5)}$ and $C_{2,q}^{(5)}$ at the EW scale $\mu_{scale} = m_Z$. In the region below the solid cyan line the limits are inconsistent with the validity of the EFT as described in Section 4.

where,

$$v_{min}^2 = \frac{q^2}{4\mu_T^2} = \frac{m_T E_R}{2\mu_T^2}, \quad (12)$$

represents the minimal incoming WIMP speed required to impart the nuclear recoil energy E_R . Moreover, in Eq. (10) the $W_{Tk}^{\tau\tau'}$'s are nuclear response functions and the index k represents different effective nuclear operators, which, under the assumption that the nuclear ground state is an approximate eigenstate of P and CP , can be at most eight: following the notation in [42, 41], $k=M, \Phi'', \Phi''M, \Phi', \Sigma'', \Sigma', \Delta, \Delta\Sigma'$. The $W_{Tk}^{\tau\tau'}$'s are function of $y \equiv (qb/2)^2$, where b is the size of the nucleus. For the target nuclei T used in most direct detection experiments the functions $W_{Tk}^{\tau\tau'}$ (y), calculated using nuclear shell models, have been provided in Refs. [41, 43]. Details about the definitions of both the functions $R_k^{\tau\tau'}$'s and $W_{Tk}^{\tau\tau'}$'s can be found in [41]. In our analysis for the WIMP local density we take $\rho_{loc}=0.3 \text{ GeV/cm}^3$ and for the velocity distribution we assume a standard isotropic Maxwellian with velocity dispersion 220 km/s, truncated at an escape velocity of 550 km/s.

4. Analysis

The expected event rate of the Migdal effect of Eq. (4) is given by the product of the WIMP-nucleus scattering rate $\frac{d^2 R_{\chi T}}{dE_R dv_T}$ and of the ionization probability p_{qe}^c . As shown in Eq. (5) due to the electron emission the kinematics of the scattering rate $R_{\chi T}$ is modified compared to the elastic case. In particular Eq. (5) describes the same kinematics of inelastic DM [44], where a low-mass DM eigenstate χ upscatters to a higher-mass state χ' with mass splitting $\delta = m_{\chi'} - m_\chi$. In the case of the Migdal effect the energy E_{EM} of the emitted electron takes the place of δ . The calculation of $\frac{d^2 R_{\chi T}}{dE_R dv_T}$ can be handled in a straightforward way by the `wimp_dd_rate` routine of WimPyDD [37], that includes the argument `delta` for inelastic scattering. In particular we fixed `delta` equal to $E_{EM} \simeq E_e$, and integrated the scattering rate over the full range of the undetected nuclear scattering energy E_R .

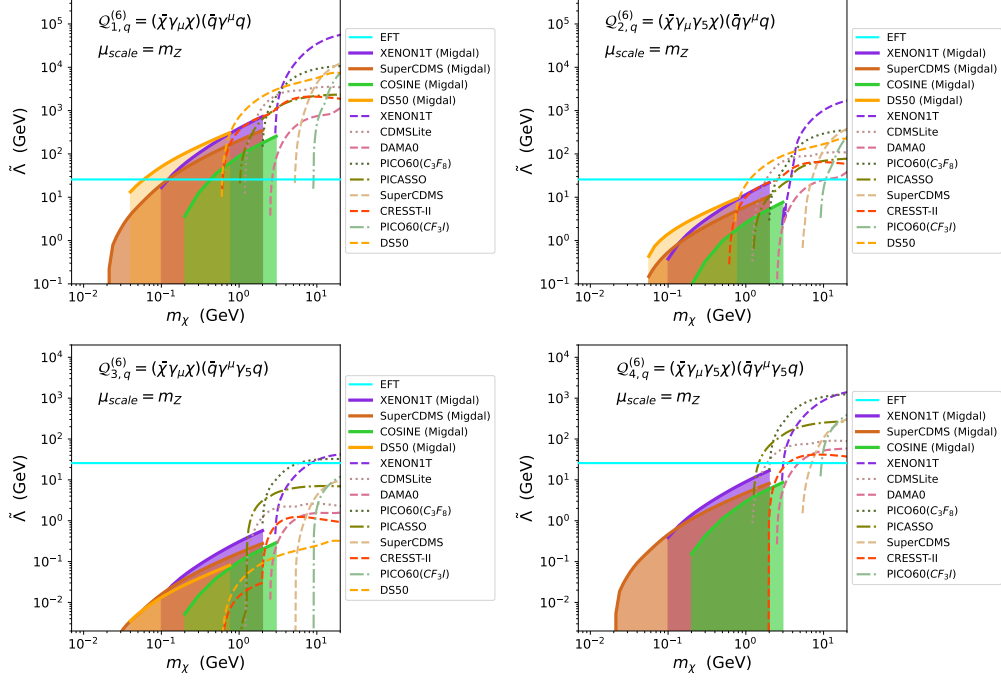


Figure 3: Same as Fig. 2 for $Q_{1,q}^{(6)}$ (top-left), $Q_{2,q}^{(6)}$ (top-right), $Q_{3,q}^{(6)}$ (bottom-left), and $Q_{4,q}^{(6)}$ (bottom-right).

Moreover, in our analysis, we fixed the dimensional couplings $C_{a,q}^{(d)}$, $C_b^{(d)}$ at the Electroweak (EW) scale $\mu_{scale} = m_Z$ and used the DirectDM [38] code to obtain the Wilson coefficients at the WIMP-nucleon interaction scale. The Wilson coefficients obtained in this way were then used in WimPyDD [37] for the calculation of WIMP-nucleus scattering rate. As for the ionisation probabilities p_{qe}^c we adopted those provided in [10] for Xenon, Sodium, Iodine, Germanium, and Argon, corresponding to the targets of XENON1T [15], COSINE-100 [16], SuperCDMS [18], and DarkSide-50 [19].

In Fig. 1 we provide one explicit example of the differential event rate for the Migdal effect in the case of a magnetic dipole interaction ($Q_1^{(5)}$) off Xe, Ge, Na, I and Ar targets. The different color shadings correspond to the ionisation rates for $n = 1, 2, 3, 4, 5$ shells. It is worth mentioning that available DD experiments are sensitive to only some of the shells (partially or fully) that contribute to the Migdal event rate, due to their energy threshold.

The results of our analysis are shown in Figs. 2, 3, 4 and 5. In particular adopting the same approach of Ref. [4] we fix the couplings $C_{a,q}^{(d)}$ to a value common to all quarks and show the constraint on each of the Wilson coefficient $C_{a,q}^{(d)}$ and $C_b^{(d)}$ of Eq. (1) in terms of a 90%–C.L. lower bound on the effective scale $\tilde{\Lambda}$ according to the parameterization of Eq.(2). In the same plots we include for completeness the corresponding constraints from the elastic recoil analysis taken from [4].

For XENON1T [15] we assume a 22 tonne-day exposure and $0.186 \leq E_{EM} \leq 3.8$ keVee, with 49 WIMP candidate events corresponding at 90% C.L. to 61 observed events and an ex-

pected background of 23.4 events.

For COSINE-100, we consider the first energy bin $1 \leq E_{EM} \leq 1.25$ keVee, with an effective exposure of 97.7 kg–year. In the same bin from the upper panel of Fig. 4 of Ref. [16] the measured count–rate is $\simeq 20000$ events, while from the lower panel the data exceed the estimated background by $\simeq 10\%$ at 90% C.L. Using this piece of information we obtain $\simeq 2000$ WIMP candidate events, which reproduce the published exclusion plot.

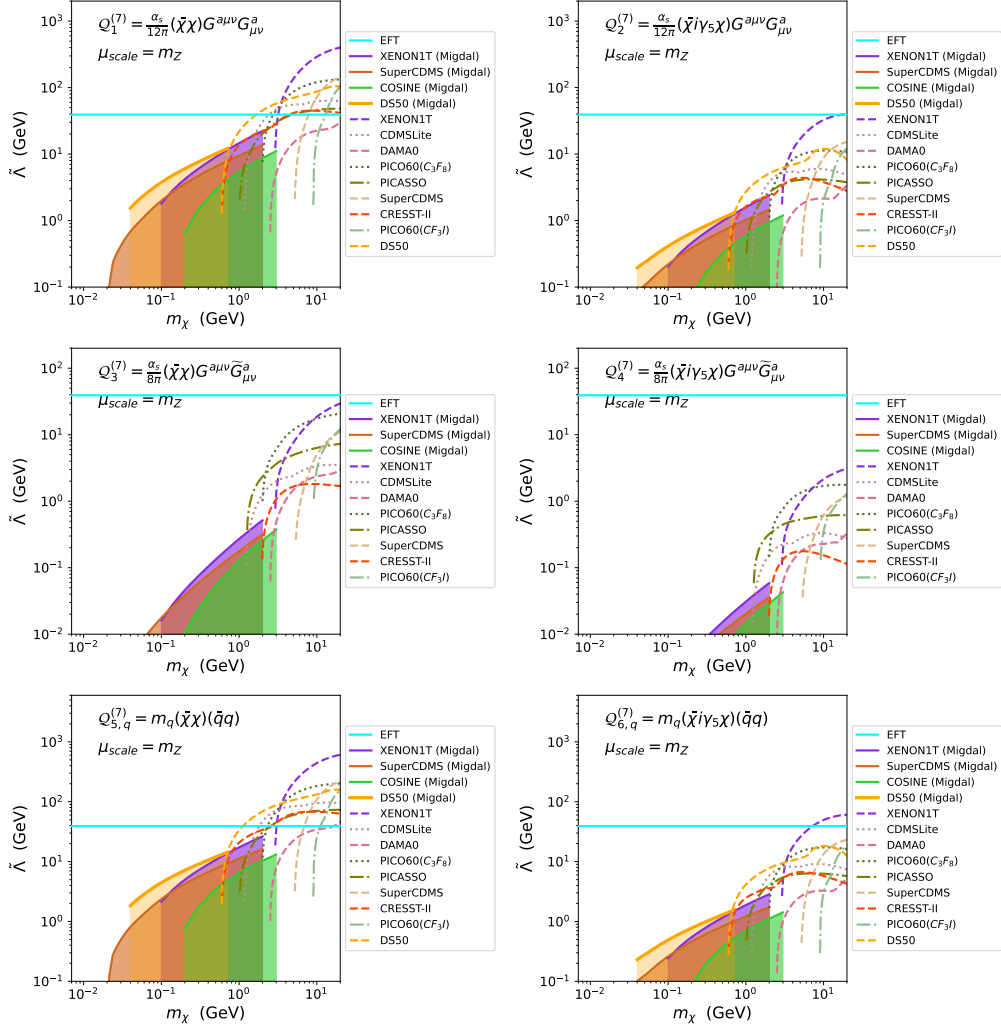


Figure 4: The same as Fig. 2 for the $Q_1^{(7)} - Q_6^{(7)}$ operators.

Recently, the SuperCDMS [18] collaboration has also published a dedicated Migdal analysis. Two separate sets of data are considered, corresponding to exposures of 18.8 kg–days and 17.5 kg–days. For both sets we consider a single energy bin $0.07 \leq E_{EM} \leq 2$ keVee, with 208 and 193 WIMP candidate events [45], respectively. In our plots we show the most constraining bound

between the two. The efficiency and resolution of SuperCDMS are taken from [45].

The profile-likelihood analysis used by DarkSide-50 [19] is difficult to reproduce, but we notice that the Migdal energy spectrum dR/dE_{EM} is fixed by the ionization probabilities p_{qe}^c and is the same for all interactions. As a consequence we directly use the normalization of the exclusion plot in [19], obtained for a standard spin-independent interaction, to estimate the upper bound on the WIMP candidate events for all other interactions. In order to reproduce the exclusion limit of Fig. 3 in Ref. [19] we adopt energy bin close to threshold, $0.083 \leq E_{EM} \leq 0.106$ keVee, where we estimate 20 events, for an exposure of $\simeq 12.5$ tonne-day.

For the sake of comparison, in Figs. 2, 3, 4 and 5 we also provide the results obtained in Ref. [4] using elastic scattering and that extend down to $m_\chi \simeq 600$ MeV. Indeed, the use of the Migdal effect allows to extend the sensitivity of DD searches to WIMP masses that are significantly lower compared to the analysis in [4], and that can reach down to $m_\chi \simeq 20$ MeV. In all the plots the experiment that is sensitive to the lowest WIMP masses is SuperCDMS, with the lowest energy threshold at 70 eV. On the other hand COSINE-100 has the higher threshold at 1 keVee and is never competitive in the determination of the constraints, with the exception of $Q_{8,q}^{(7)}$.

Figs. 2, 3, 4 and 5 can be roughly divided in two classes: in the case of operators $Q_{1,q}^{(5)}$, $Q_{2,q}^{(5)}$, $Q_{1,q}^{(6)}$, $Q_{2,q}^{(6)}$, $Q_1^{(7)}$, $Q_2^{(7)}$, $Q_{5,q}^{(7)}$, $Q_{6,q}^{(7)}$ and $Q_{10,q}^{(7)}$ the scattering cross section is driven in the non-relativistic limit by the W_M nuclear response function, which corresponds to a coherent spin-independent interaction. In this case for $m_\chi \gtrsim 40$ MeV DarkSide-50 is the most constraining experiment, while the constraint from XENON1T starts at $m_\chi \simeq 100$ MeV and reaches the same sensitivity of DarkSide-50 at $m_\chi \simeq 1$ GeV.

A second class of exclusion plots is represented by the operators $Q_{3,q}^{(6)}$, $Q_{4,q}^{(6)}$, $Q_3^{(7)}$, $Q_4^{(7)}$, $Q_{7,q}^{(7)}$, $Q_{8,q}^{(7)}$, and $Q_{9,q}^{(7)}$, for which, instead, in the non-relativistic limit the scattering cross section is driven by a nuclear response function of the spin-dependent type (either Σ'' , Σ' or both). In this case the DarkSide-50 bound is not present because Argon (^{40}Ar) has no spin, so that for $m_\chi \gtrsim 100$ MeV XENON1T is the most constraining bound. One exception is represented by the $Q_{3,q}^{(6)}$ operator that develops a $Q_{1,q}^{(6)}$ component driven by the W_M nuclear response function in the running from m_Z to the nucleon scale [46, 47]. This leads to a non-vanishing bound from DarkSide-50 for $m_\chi \gtrsim 40$ MeV, that turns out to be at the same level of XENON1T. Some of the limits shown in Figs. 2, 3, 4 and 5 may be so weak that they put bounds on values of the $\tilde{\Lambda}$ scale which are inconsistent with the validity of the effective theory. In such case one can simply conclude that the present experimental sensitivity of direct detection experiments is not able to put bounds on the corresponding effective operator. A possible (but not unique) criterion for the validity of the EFT is the same that we adopted in Ref. [4]. In this case the scale $\tilde{\Lambda}$ is interpreted in terms of a propagator g^2/M_*^2 with $g < \sqrt{4\pi}$ and $M_* > \mu_{scale}$, with $\mu_{scale} = m_Z$ the scale were we fixed the boundary conditions of the EFT. This is straightforward for dimension-6 operators, while in the case of operators whose effective coupling has dimension different from -2 only matching the EFT with the full theory would allow to draw robust conclusions. In particular, in this case $\tilde{\Lambda}$ can be interpreted in terms of the same propagator times the appropriate power of a typical scale of the problem μ'_{scale} , which depends on the ultraviolet completion of the EFT. For instance, in the operator $Q_{5,q}^{(7)} = m_q (\bar{\chi}\chi)(\bar{q}q)$ the quark mass may originate from a Yukawa coupling, so μ'_{scale} corresponds to the Electroweak vacuum expectation value. To fix an order of magnitude we choose to fix $\mu'_{scale} = \mu_{scale}$, so that the bound $\tilde{\Lambda} > \mu_{scale}/(4\pi)^{1/(d-4)}$ can be derived. Such limit is shown as a horizontal solid line in Figs. 2, 3, 4 and 5. In particular, for models $Q_3^{(6)}$, $Q_4^{(6)}$ in Fig. 3

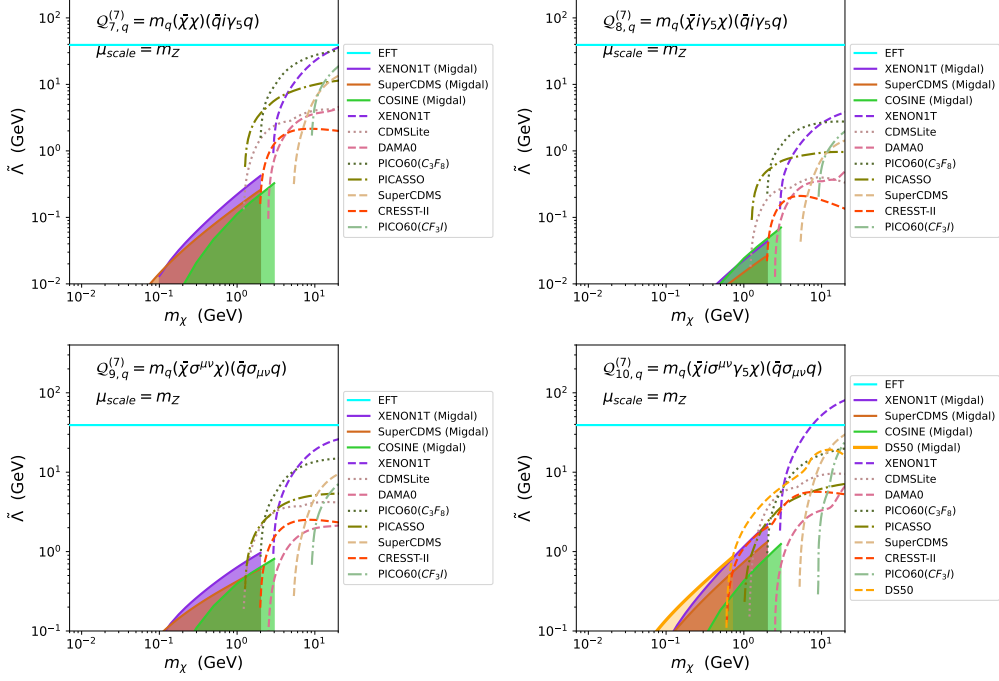


Figure 5: The same as Fig. 2 for the $Q_7^{(7)} - Q_{10}^{(7)}$ operators.

and for all the dimension-7 operators of Figs. 4 and 5 the extension at low WIMP masses of the exclusion plot on the $\tilde{\Lambda}$ scale obtained with our Migdal effect analysis lies below such horizontal line. This may imply that the sensitivities of the present direct detection experiments optimized to search for the Migdal effect is not sufficient to put meaningful bounds at low WIMP masses. However we stress again that this can only be assessed when a specific ultraviolet completion of the effective theory is assumed.

5. Conclusion

In a previous analysis [4] we studied the direct detection bounds from elastic WIMP–nucleus scattering to operators up to dimension 7 of the relativistic effective field theory describing WIMP interactions with quarks and gluons. Such bounds reached a WIMP mass $m_\chi \gtrsim 600$ MeV. In the present letter we have used the inelastic Migdal effect, where the recoiling nucleus is ionized, to extend such bounds to lower WIMP masses. In particular, analyzing the data of XENON1T, SuperCDMS, COSINE-100, and DarkSide-50 we find that the bounds can reach down to a WIMP mass $\simeq 20$ MeV. In the case of higher–dimension operators the energy scale of the ensuing constraints may be inconsistent with the validity of the effective theory.

Acknowledgements

The work of G.T. was supported by the Collaborative Research Center SFB1258. The work of S.K. and S.S. was supported by the National Research Foundation of Korea (NRF) funded by the Ministry of Education through the Center for Quantum Space Time (CQUeST) with grant number 2020R1A6A1A03047877 and by the Ministry of Science and ICT with grant number 2021R1F1A1057119. G.T is thankful to Alejandro Ibarra and Maximilian Gapp for helpful discussions.

References

- [1] M. Schumann, *Direct Detection of WIMP Dark Matter: Concepts and Status*, *J. Phys. G* **46** (2019) 103003, [1903.03026].
- [2] R. K. Leane et al., *Snowmass2021 Cosmic Frontier White Paper: Puzzling Excesses in Dark Matter Searches and How to Resolve Them*, 2203.06859.
- [3] F. Bishara, J. Brod, B. Grinstein and J. Zupan, *From quarks to nucleons in dark matter direct detection*, *JHEP* **11** (2017) 059, [1707.06998].
- [4] S. Kang, S. Scopel, G. Tomar and J.-H. Yoon, *On the sensitivity of present direct detection experiments to WIMP–quark and WIMP–gluon effective interactions: A systematic assessment and new model–independent approaches*, *Astropart. Phys.* **114** (2020) 80–91, [1810.00607].
- [5] J. D. Vergados and H. Ejiri, *The role of ionization electrons in direct neutralino detection*, *Phys. Lett. B* **606** (2005) 313–322, [hep-ph/0401151].
- [6] C. C. Moustakidis, J. D. Vergados and H. Ejiri, *Direct dark matter detection by observing electrons produced in neutralino-nucleus collisions*, *Nucl. Phys. B* **727** (2005) 406–420, [hep-ph/0507123].
- [7] H. Ejiri, C. C. Moustakidis and J. D. Vergados, *Dark matter search by exclusive studies of X-rays following WIMPs nuclear interactions*, *Phys. Lett. B* **639** (2006) 218–222, [hep-ph/0510042].
- [8] J. D. Vergados, H. Ejiri and K. G. Savvidy, *Theoretical direct WIMP detection rates for inelastic scattering to excited states*, *Nucl. Phys. B* **877** (2013) 36–50, [1307.4713].
- [9] R. Bernabei et al., *On electromagnetic contributions in WIMP quests*, *Int. J. Mod. Phys. A* **22** (2007) 3155–3168, [0706.1421].
- [10] M. Ibe, W. Nakano, Y. Shoji and K. Suzuki, *Migdal Effect in Dark Matter Direct Detection Experiments*, *JHEP* **03** (2018) 194, [1707.07258].
- [11] A. Migdal, *Ionization of atoms accompanying α - and β -decay*, *J. Phys. USSR* **4** (1941) 449.
- [12] LUX collaboration, D. S. Akerib et al., *Results of a Search for Sub-GeV Dark Matter Using 2013 LUX Data*, *Phys. Rev. Lett.* **122** (2019) 131301, [1811.11241].
- [13] EDELWEISS collaboration, E. Armengaud et al., *Searching for low-mass dark matter particles with a massive Ge bolometer operated above-ground*, *Phys. Rev. D* **99** (2019) 082003, [1901.03588].
- [14] CDEX collaboration, Z. Z. Liu et al., *Constraints on Spin-Independent Nucleus Scattering with sub-GeV Weakly Interacting Massive Particle Dark Matter from the CDEX-1B Experiment at the China Jinping Underground Laboratory*, *Phys. Rev. Lett.* **123** (2019) 161301, [1905.00354].
- [15] XENON collaboration, E. Aprile et al., *Search for Light Dark Matter Interactions Enhanced by the Migdal Effect or Bremsstrahlung in XENON1T*, *Phys. Rev. Lett.* **123** (2019) 241803, [1907.12771].
- [16] COSINE-100 collaboration, G. Adhikari et al., *Searching for low-mass dark matter via the Migdal effect in COSINE-100*, *Phys. Rev. D* **105** (2022) 042006, [2110.05806].
- [17] EDELWEISS collaboration, E. Armengaud et al., *Search for sub-GeV Dark Matter via Migdal effect with an EDELWEISS germanium detector with NbSi TES sensors*, 2203.03993.
- [18] SUPERCDMS collaboration, M. Al-Bakry et al., *A Search for Low-mass Dark Matter via Bremsstrahlung Radiation and the Migdal Effect in SuperCDMS*, 2203.02594.
- [19] DARKSIDE collaboration, P. Agnes et al., *Search for dark matter-nucleon interactions via Migdal effect with DarkSide-50*, 2207.11967.
- [20] M. J. Dolan, F. Kahlhoefer and C. McCabe, *Directly detecting sub-GeV dark matter with electrons from nuclear scattering*, *Phys. Rev. Lett.* **121** (2018) 101801, [1711.09906].
- [21] R. Essig, J. Pradler, M. Sholapurkar and T.-T. Yu, *Relation between the Migdal Effect and Dark Matter-Electron Scattering in Isolated Atoms and Semiconductors*, *Phys. Rev. Lett.* **124** (2020) 021801, [1908.10881].
- [22] G. Grilli di Cortona, A. Messina and S. Piacentini, *Migdal effect and photon Bremsstrahlung: improving the sensitivity to light dark matter of liquid argon experiments*, *JHEP* **11** (2020) 034, [2006.02453].

- [23] V. V. Flambaum, L. Su, L. Wu and B. Zhu, *Constraining sub-GeV dark matter from Migdal and Boosted effects*, 2012.09751.
- [24] S. Knapen, J. Kozaczuk and T. Lin, *Migdal Effect in Semiconductors*, *Phys. Rev. Lett.* **127** (2021) 081805, [2011.09496].
- [25] U. K. Dey, T. N. Maity and T. S. Ray, *Prospects of Migdal Effect in the Explanation of XENONIT Electron Recoil Excess*, *Phys. Lett. B* **811** (2020) 135900, [2006.12529].
- [26] N. F. Bell, J. B. Dent, B. Dutta, S. Ghosh, J. Kumar and J. L. Newstead, *Low-mass inelastic dark matter direct detection via the Migdal effect*, *Phys. Rev. D* **104** (2021) 076013, [2103.05890].
- [27] N. F. Bell, J. B. Dent, R. F. Lang, J. L. Newstead and A. C. Ritter, *Observing the Migdal effect from nuclear recoils of neutral particles with liquid xenon and argon detectors*, *Phys. Rev. D* **105** (2022) 096015, [2112.08514].
- [28] W. Wang, K.-Y. Wu, L. Wu and B. Zhu, *Direct Detection of Spin-Dependent Sub-GeV Dark Matter via Migdal Effect*, 2112.06492.
- [29] Z.-L. Liang, C. Mo, F. Zheng and P. Zhang, *A phonon-mediated description of the Migdal effect in semiconductor detectors*, 2205.03395.
- [30] S. Chatterjee and R. Laha, *Explorations of pseudo-Dirac dark matter having keV splittings and interacting via transition electric and magnetic dipole moments*, 2202.13339.
- [31] J. R. Angevaere, G. Bertone, A. P. Colijn, M. P. Decowski and B. J. Kavanagh, *Complementarity of direct detection experiments in search of light Dark Matter*, 2204.01580.
- [32] P. Cox, M. J. Dolan, C. McCabe and H. M. Quiney, *Precise predictions and new insights for atomic ionisation from the Migdal effect*, 2208.12222.
- [33] N. F. Bell, J. B. Dent, J. L. Newstead, S. Sabharwal and T. J. Weiler, *Migdal effect and photon bremsstrahlung in effective field theories of dark matter direct detection and coherent elastic neutrino-nucleus scattering*, *Phys. Rev. D* **101** (2020) 015012, [1905.00046].
- [34] R. Bernabei, P. Belli, F. Cappella, R. Cerulli, F. Montecchia, F. Nozzoli, A. Incicchitti, D. Prosperi, C. J. Dai and H. H. Kuang, *et al.* *Riv. Nuovo Cim.* **26N1**, 1-73 (2003) [arXiv:astro-ph/0307403 [astro-ph]].
- [35] I. Coarasa, J. Amaré, S. Cebrián, C. Cuesta, E. García, M. Martínez, M. A. Oliván, Y. Ortigoza, A. Ortiz de Solórzano and J. Puimedón, *et al.* *Eur. Phys. J. C* **79**, no.3, 233 (2019) doi:10.1140/epjc/s10052-019-6733-4 [arXiv:1812.02000 [astro-ph.IM]].
- [36] Y. J. Ko *et al.* [COSINE-100], *JCAP* **11**, 008 (2019) doi:10.1088/1475-7516/2019/11/008 [arXiv:1907.04963 [hep-ex]].
- [37] I. Jeong, S. Kang, S. Scopel and G. Tomar, *WimPyDD: An object-oriented Python code for the calculation of WIMP direct detection signals*, *Comput. Phys. Commun.* **276** (2022) 108342, [2106.06207].
- [38] F. Bishara, J. Brod, B. Grinstein and J. Zupan, *DirectDM: a tool for dark matter direct detection*, 1708.02678.
- [39] E. Del Nobile, *Complete Lorentz-to-Galileo dictionary for direct dark matter detection*, *Phys. Rev.* **D98** (2018) 123003, [1806.01291].
- [40] S. Kang, S. Scopel, G. Tomar and J.-H. Yoon, *Present and projected sensitivities of Dark Matter direct detection experiments to effective WIMP-nucleus couplings*, *Astropart. Phys.* **109** (2019) 50–68, [1805.06113].
- [41] N. Anand, A. L. Fitzpatrick and W. C. Haxton, *Weakly interacting massive particle-nucleus elastic scattering response*, *Phys. Rev.* **C89** (2014) 065501, [1308.6288].
- [42] A. L. Fitzpatrick, W. Haxton, E. Katz, N. Lubbers and Y. Xu, *The Effective Field Theory of Dark Matter Direct Detection*, *JCAP* **1302** (2013) 004, [1203.3542].
- [43] R. Catena and B. Schwabe, *Form factors for dark matter capture by the Sun in effective theories*, *JCAP* **1504** (2015) 042, [1501.03729].
- [44] D. Tucker-Smith and N. Weiner, *Inelastic dark matter*, *Phys. Rev.* **D64** (2001) 043502, [hep-ph/0101138].
- [45] SUPERCDMS collaboration, R. Agnese *et al.*, *Search for Low-Mass Dark Matter with CDMSlite Using a Profile Likelihood Fit*, *Phys. Rev. D* **99** (2019) 062001, [1808.09098].
- [46] F. D’Eramo and M. Procura, *Connecting Dark Matter UV Complete Models to Direct Detection Rates via Effective Field Theory*, *JHEP* **04** (2015) 054, [1411.3342].
- [47] F. D’Eramo, B. J. Kavanagh and P. Panci, *You can hide but you have to run: direct detection with vector mediators*, *JHEP* **08** (2016) 111, [1605.04917].